ELSEVIER

Powder Technology 91 (1997) 83–93

POWDER TECHNOLOGY

Tensile strength of wet granular materials

Patrice Pierrat, Hugo S. Caram *

Chemical Engineering Department, Lehigh University, Bethlehem, PA 18015, USA

Received 8 August 1994; revised 19 December 1995

Abstract

The dimensionless tensile strength $\sigma d/\alpha$ of wet granular materials with saturation levels in the plateau region of the pendular state was correlated with the void fraction of the agglomerate. The correlation fitted well with experimental measurements carried out on glass beads of diameter 93 μm and with literature data, and was an improvement over the traditional Rumpf model. The tensile strength at other saturations could be easily derived from the proposed correlation. The effects of bed height in the tester cell, liquid saturation levels in the agglomerate, chemical additives and non-uniformity of the packing of the powder mass were also investigated.

Keywords: Characterization; Wet solids; Tensile strength

1. Introduction

Tensile strength is an important parameter in powder characterization. It can also be combined with the yield locus of a wet granular material to characterize its flow properties. The tensile strength of wet powders can be measured directly by means of testing apparatuses available on the market [1–7]. However, it would be of considerable interest to predict its value from easy-to-measure parameters such as void fraction, particle size, etc. A simple model is introduced and compared with tensile strength measurements on wet glass beads. Finally, a new correlation is proposed, allowing for the calculation of the tensile strength of any wet granular material.

2. Adhesion force due to a liquid bridge

2.1. Forces acting in a liquid bridge

The interaction between the liquid and the solid in wet granular materials depends on the amount of liquid present. A small quantity of liquid causes liquid bridges to form between the particles of the agglomerate. This state is called the 'pendular state'. By increasing the amount of liquid, the 'funicular state' is obtained where both liquid bridges and pores filled with liquid are present. The 'capillary state' is reached when all the pores are filled with the liquid and

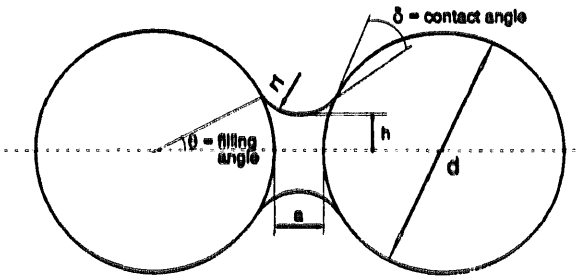

Fig. 1. Liquid bridge bonding two monosized particles.

concave menisci develop at the surface of the agglomerate. In the pendular state, the maximum tensile force transmitted by a liquid bridge bonding two monosized spherical particles of diameter d and separated by a distance a (Fig. 1) consists of two components. The first, F_s, is due to the surface tension of the liquid at the liquid–particle contact line and is given in dimensionless form as

$$\frac{F_s}{\alpha d} = \pi \sin\theta \sin(\theta+\delta) \tag{1}$$

where θ is the filling angle, and α and δ are the surface tension and contact angle, respectively, of the wetting liquid.

The second, F_c, is due to the curvature of the liquid bridge which creates a pressure difference across the surface:

$$\frac{F_c}{\alpha d} = \pi\left(\frac{\sin\theta}{2}\right)^2\left(\frac{1}{r_1^*}-\frac{1}{h^*}\right) \tag{2}$$

with

* Corresponding author.

0032-5910/97/$17.00 © 1997 Published by Elsevier Science S.A. All rights reserved
PII S0032-5910(96)03179-8

$$h^* = \frac{h}{d} = \frac{\sin\theta}{2} + \frac{r_1}{d}\left[\sin(\theta+\delta) - 1\right] \quad (3)$$

$$r_1^* = \frac{r_1}{d} = \frac{(1-\cos\theta) + a/d}{2\cos(\theta+\delta)} \quad (4)$$

where h^* and r_1^* are the two dimensionless radii of curvature of the liquid bridge when taken as arcs of a circle. The exact values of the radii of curvature h and r_1 can be obtained by solving numerically the Laplace Young equation for the surface shape. However, Heady and Cahn [8] compared the rigorous solution with the one based on the circle approximation and showed that the error was very small in practice.

The total dimensionless force is the sum of the two components:

$$\frac{F_t}{\sigma d} = \pi \sin\theta\left[\sin(\theta+\delta) + \frac{\sin\theta}{4}\left(\frac{1}{r_1^*} - \frac{1}{h^*}\right)\right] \quad (5)$$

Combining Eqs. (3), (4) and (5), one can see that the dimensionless bonding force is only a function of the contact and filling angles and the dimensionless separation distance. The filling angle is determined by the moisture content x_w, defined as the ratio of the mass of liquid to the mass of dry particles. It is given by the following relation:

$$x_w = \frac{m_{liq}}{m_{sol}} = \frac{V_{liq}\rho_{liq}}{V_{sol}\rho_{sol}} = \frac{k(V_{bridge}/2)}{\pi d^3/6}\frac{\rho_{liq}}{\rho_{sol}} = 6k\left(\frac{V_{bridge}}{2\pi d^3}\right)\frac{\rho_{liq}}{\rho_{sol}} \quad (6)$$

where k is the mean number of contact points per particle or the mean coordination number, V_{bridge} is the volume of the liquid bridge, and ρ_{liq} and ρ_{sol} are the liquid and particle densities, respectively. There are several models, reviewed by Mehrotra and Sastry [9], for the calculation of the liquid bridge volume. Pietsch and Rumpf [10] gave the following expression, assuming r_1 to be a constant:

$$\frac{V_{bridge}}{2\pi d^3} = \left[r_1^{*2} + (r_1^* + h^*)^2\right] r_1^* \cos(\theta+\delta) - \frac{r_1^{*3}\cos^3(\theta+\delta)}{3} - r_1^{*2}(r_1^* + h^*) \times\left[\cos(\theta+\delta)\sin(\theta+\delta)\left(\frac{\pi}{2} - \theta - \delta\right)\right] - \frac{1}{24}(2+\cos\theta)(1-\cos\theta)^2 \quad (7)$$

Fig. 2 shows a plot of the contributing dimensionless forces and the resulting dimensionless force as a function of the filling angle for a dimensionless separation distance $a/d = 0.025$ and complete wetting ($\delta = 0°$). As the filling angle increases, so does the length of the liquid–solid contact line and the attraction force which is the product of this length with the surface tension of the wetting liquid. The force due to the curvature of the bridge as a function of the filling angle θ goes through a maximum, then starts decreasing, and eventually becomes negative, indicating a repulsive force. This trend is due to the relative size of the two dimensionless radii

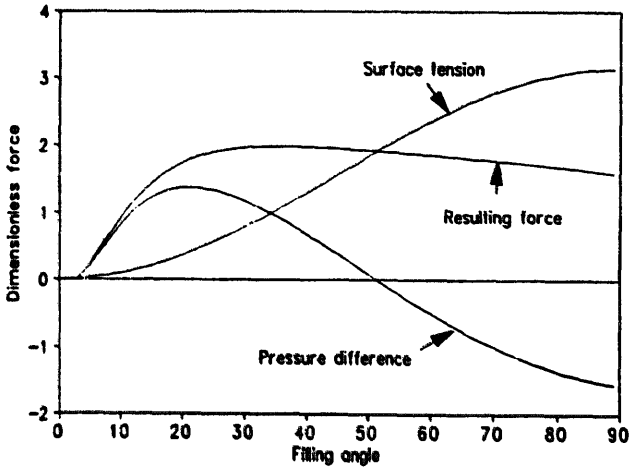

Fig. 2. Dimensionless force as a function of the filling angle ($a/d = 0.025$ and $\delta = 0°$).

of curvature h^* and r_1^*. At low filling angles, r_1^* is smaller than h^*. As the size of the liquid bridge grows, h^* increases faster than r_1^* and eventually becomes larger. The net resulting force is a positive (attraction) force that increases sharply with moisture content at low filling angles and levels off to a plateau as the moisture is further increased.

2.2. Effect of the separation distance

The separation distance a between particles has an effect on the magnitude of the attraction force. Fig. 3 shows different profiles for the dimensionless attraction force calculated for $\delta = 0°$ and for different values of the dimensionless separation distance a/d. The largest force occurs between two touching particles ($a/d = 0$) and the force decreases as the distance between particles increases. Because, in practice, no absolutely smooth particles are found, the case $a/d = 0$ seldom occurs in a real agglomerate. Instead, values of a/d in the range 0.005–0.05 are more appropriate and seem to correlate the experimental data well; the value $a/d = 0.025$ was used in this paper.

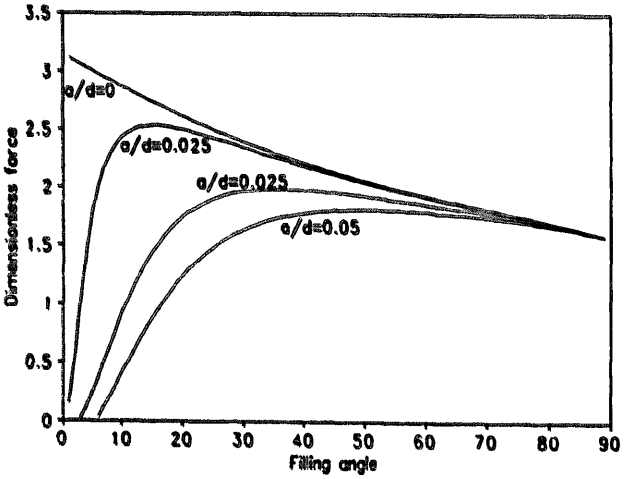

Fig. 3. Effect of the separation distance on the dimensionless bonding force for $\delta = 0°$.

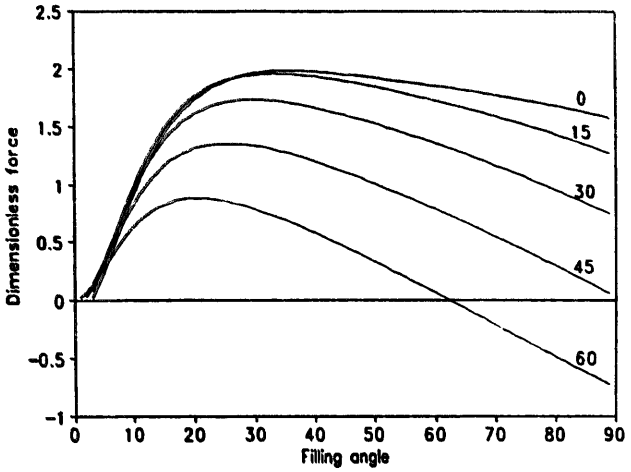

Fig. 4. Effect of the contact angle on the dimensionless bonding force for $a/d = 0.025$.

2.3. Effect of the contact angle

The effect of the contact angle of the wetting liquid is shown in Fig. 4. As the contact angle increases, the dimensionless attraction force decreases. Discrepancies with the force calculated at $\delta = 0°$ are small for values of δ up to 25° but become larger as the contact angle increases. The calculations were done for $a/d = 0.025$.

3. Tensile strength of wet granular materials

There are several correlations for the tensile strength of wet powders. Schubert [11] reviews different models which are globally of the same form, only differing in the fitting parameters. Among these correlations, it appears that the general formulae derived by Rumpf [12] are widely accepted. His model is based on the following assumptions. First, all the particles are monosized spheres statistically (on the average uniformly) distributed in the agglomerate. Second, the bonds are statistically distributed across the surface and over the directions in space. Finally, the effective bonding forces are distributed around a mean value which can be used in the calculations. Rumpf gave the following expression for the tensile strength σ_{pz} of wet powders in the pendular state:

$$\sigma_{pz} = (1-\epsilon)\frac{k}{\pi}\frac{F_t}{d^2} \tag{8}$$

where ϵ is the void fraction of the agglomerate and F_t the bonding force of the liquid bridges given by Eq. (5). The coordination number k is a function of the packing density or the void fraction of the bulk. Several empirical correlations are reported in the literature and are based on packing experiments of monosized particles. Rumpf [13] used the results of Smith et al. [14] and proposed

$$k\epsilon = \pi \tag{9}$$

With this assumption, the expression for the tensile strength of wet granular material in the pendular region is

$$\sigma_{pz} = \frac{1-\epsilon}{\epsilon}\frac{\pi\alpha}{d}\sin\theta\left[\sin(\theta+\delta) + \frac{\sin\theta}{4}\left(\frac{1}{r_1^*} - \frac{1}{h^*}\right)\right] \tag{10}$$

In the capillary state where all the pores are completely filled with the liquid, the interfacial forces exist only at the surface of the agglomerate and a negative capillary pressure p_c develops in the interior, holding the particles together. In this case, the tensile strength is given by Schubert [15] as

$$\sigma_{cz} = Sp_c \tag{11}$$

where p_c is the capillary pressure:

$$p_c = a'\frac{1-\epsilon}{\epsilon}\frac{\alpha}{d} \tag{12}$$

with a' taking values between 6 and 8. S is the saturation amount, defined as the ratio of the void volume occupied by the liquid to the total void volume. The saturation amount is related to the moisture content calculated on a dry basis by the following relation:

$$S = \frac{1-\epsilon}{\epsilon}\frac{\rho_{sol}}{\rho_{liq}}x_w \tag{13}$$

In the funicular state, Schubert [16] proved experimentally that both ridge bonding and bonding caused by regions filled with liquid contribute to the strength of the agglomerate. The tensile strength a_{fz} in this region is a linear combination of σ_{pz} and σ_{cz}:

$$\sigma_{fz} = \sigma_{pz}\frac{S_c - S}{S_c - S_f} + \sigma_{cz}\frac{S - S_f}{S_c - S_f} \tag{14}$$

where S_c and S_f are the upper saturation limits for the funicular and pendular states, respectively.

The capillary state usually occurs for saturation levels greater than 90% ($S_c \geq 0.9$). S_f is a function of the moisture content and the packing density of the agglomerate. Flemmer [17] gave a method based on geometrical considerations to determine its value. He found that, for randomly packed equal-size particles, $S_f = 34\%$. Usually, for the range of void fractions considered, the limit is between 25 and 50%.

4. Experimental measurements of tensile strength

4.1. Apparatus and material used

The split cell tester developed by Hartley and Parfitt [5] was used in this work and is shown in Fig. 5. The apparatus, originally designed for the measurement of the tensile strength of very fine cohesive powders, uses a small split cell 25 mm in diameter and 6 mm in height. A larger cell (inside diameter 81 mm, height 25 mm) was built in order to perform tensile strength measurements on weakly cohesive powders. The testing procedure is as follows. The two halves of the split cell are clamped together. The material to be tested is spooned into the cell and consolidated using a piston of the

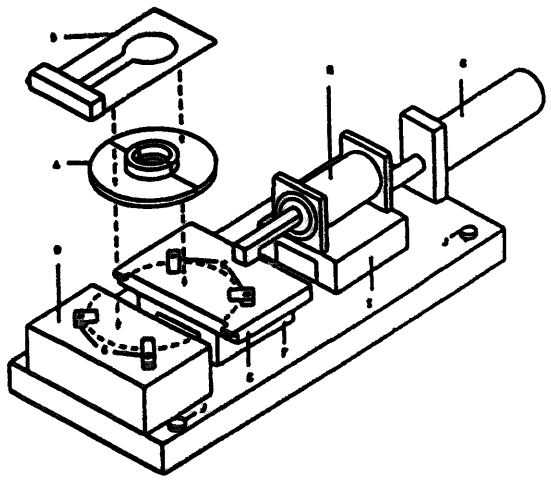

Fig. 5. Parfitt tensile strength tester: A, split cell; B, clamp; C, positioning clamps; D, fixed base; E, movable base; F and I, ball bearings; G, inchworm translator; H, force transducer.

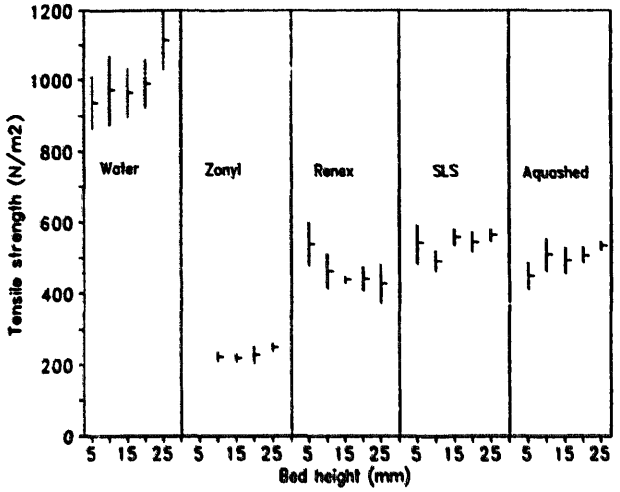

Fig. 6. Measured tensile strength as a function of the bed height in the cell (saturation = 12% and $\epsilon = 0.438$).

Table 1
Surface tension of the wetting liquids

Wetting solution	Renex	Aquashed	SLS	Zonyl	Water
Surface tension (N/m)	0.020	0.032	0.0347	0.0384	0.072

same diameter as the inside diameter of the cell. Some twists are applied to the piston so the particles can rearrange and reorientate themselves, breaking any air pockets that could be present in the bulk. Once the cell is filled, it is fastened on the split base and the clamp is removed. The translator is turned on, pulling the half of the base that is resting on ball bearings. The force needed to fracture the sample is measured by a force transducer and recorded. The tensile strength is obtained by calculating the ratio of the fracture force to the cross-sectional area of the sample in the cell. Experiments were carried out on glass beads of average diameter 93 μm with a density of 2.46 g/cm^3. The samples were tested at different moisture contents corresponding to different saturation levels in the pendular region and wetted with water and different surfactants. The surfactants used with their surface tensions in solution with water are given in Table 1. The contact angles of the solutions with the glass beads were taken to be equal to zero.

4.2. *Effect of the bed height*

Schubert [11], who conducted some tensile strength measurements on wet powders with a split-cell apparatus of his own design, found that the height of the bed in the cell affects the value of the measured tensile strength. He stated that the elongation of the material responsible for the tensile resistance in the vicinity of the slit in the plate decreases towards the top surface of the material where the stress is smaller. Therefore, an increase in the height of the sample does not contribute to the fracture force that must be applied, but only increases the cross-sectional area, leading to a smaller tensile force per unit area. He recommended that several measurements should be performed at different sample heights, extrapolating to zero height to determine the actual tensile strength. Zero height corresponds to the location where the fracture initiates before propagating upwards through the bed. Fig. 6 shows the measured values of the tensile strength of glass beads wetted with different solutions as a function of the height of the bed in the cell. The experiments were carried out on samples at a saturation of 12% and with a void fraction of 0.438. Eight measurements were performed for each of the five bed heights considered and the recorded tensile forces were averaged and divided by the fracture plane area to give the tensile strength. The horizontal bars represent the average values and the vertical bars indicate the 95% confidence intervals. Contrary to Schubert's observations, the tensile strength did not increase as the bed height decreased except for samples wetted with the Renex (ICI Surfactants, Wilmington, DE) solution. For water and the Aquashed (Chemlink, Allison Park, PA) solution, the tensile strength seemed to decrease with the bed height. The SLS (SAF Bulk Chemicals, Saint Louis, MO) and Zonyl (Dupont, Wilmington, DE) solutions exhibited constant values. For samples wetted with Zonyl, measurements could not be done at bed heights less than 10 mm because the recorded tensile force was too small and very inconsistent. Overall, reproducibility of the measurements was good since the 95% confidence interval was no more than 10% of the average value. As a general trend, if one measurement at one bed height is disregarded for each sample wetted with the five different solutions, the tensile strength seems to be constant, indicating that it does not vary with the bed height. Consequently, extrapolation to zero height should not be necessary and measurements at one selected bed height should be sufficient to determine the tensile strength of the powder investigated. As shown later, the results obtained here are also supported by the measurements of the tensile strength of samples with mixed void fractions. In the later experiments, tests were performed on samples with a compacted bed height of 20 mm.

Table 2
Comparison of the ratios of tensile strengths and surface tensions

Wetting solution	Water	Zonyl	Renex	Aquashed	SLS
$\sigma_{z\,av}$ (N/m^2)	1007.6	229.4	467.4	496.0	531.2
$\sigma_{z\,sol}/\sigma_{z\,water}$	1	0.228	0.464	0.492	0.527
$\alpha_{sol}/\alpha_{water}$	1	0.278	0.444	0.482	0.533

4.3. Effect of additives on the tensile strength

Since the tensile strength is not a function of the bed height, the average tensile strength $\sigma_{z\,av}$ for each wetting liquid was calculated from all the measurements at different heights. In order to verify the proportionality of the tensile strength to the surface tension of the wetting liquid, the computed average values $\sigma_{z\,sol}$ were divided by the average value of the tensile strength $\sigma_{z\,water}$ of the powder wetted with water and compared with the ratio of the surface tension of the wetting liquid, α_{sol}, to that of water, α_{water}. The results are given in Table 2. As expected from Eq. (10), the results show the proportionality between the tensile strength and the surface tension of the wetting liquid since the calculated ratios are almost identical and the discrepancies within experimental error.

4.4. Effect of saturation on the tensile strength

Experiments were conducted on samples at different saturation levels, kept under 30% in order to stay in the pendular region. Water was the wetting liquid and the void fraction of the bed inside the cell was $\epsilon = 0.45$. The measured values of the tensile strength are shown in Fig. 7. The vertical bars represent the 95% confidence interval and the squares correspond to the average values calculated from eight measurements. Curves representing the predicted values calculated from Eq. (10) are also drawn for comparison. These curves are calculated for dimensionless separation distances of 0.035 and 0.09. It can be seen that the model overpredicts the experimental measurements for $a/d = 0.035$ corresponding to a separation distance of 3.3 μm. The difference between the data and the curve is nearly constant over the saturation range and is off by a factor of 180%. However, the experimental data follow the expected trend with a sharp increase of the tensile strength at low saturation and a plateau value for saturations greater than 20%. For a larger separation distance of 8.4 μm ($a/d = 0.09$), the curve lies closer to the experimental points but it does not really fit the data. Also, in this case the curvature is not appropriate since it does not show a sharp increase of the tensile strength at low saturations and does not level off to a plateau value at higher saturations. Other attempts to fit the data using larger separation distances in the calculations moved the curves downward and made them lie closer to the experimental points at high saturations. However, at lower saturations they failed to fit the data. Also, the liquid bridge collapses and no longer exists for separation distances that are too large.

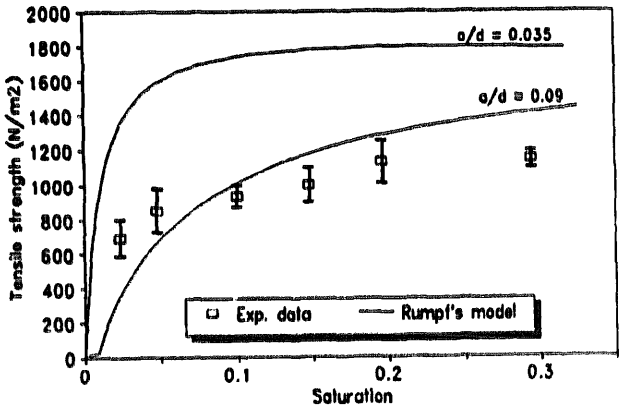

Fig. 7. Tensile strength as a function of saturation for glass beads 93 μm in diameter and a void fraction of 0.45: comparison with Rumpf's model.

4.5. Comparison of Rumpf's model with experimental data

The data from Schubert [11] for limestone particles 71 μm in diameter agrees well with the values predicted by Rumpf's model for $a/d = 0.035$. However, for the same value of the dimensionless separation distance, Rumpf's model overpredicts the experimental data of other workers [6,18–20]. In almost all cases, the experimental data show the right trend with a sharp increase of the tensile strength at low saturation and a plateau region at higher saturations in the pendular state. When a larger dimensionless separation distance is used in the computations, the curve is shifted downwards, closer to the experimental data, but the general trend is not good since in this case the curve does not level off to a constant value.

Shinohara and Tanaka [6] postulated that the discrepancies between measured and predicted values can be due to an uneven packing of the powder mass and, therefore, the ultimate tensile strength obtained is much less than that of the uniformly packed powder mass assumed by Rumpf. In addition, the experimental relationship between the coordination number and the void fraction given by Eq. (9) does not always hold over a wide range of void fractions. They claim that a unit cross-sectional area of powder is composed of two kinds of regular packing portions of equivalent spheres (cubic packing and rhombohedral packing). Since each particle in the rhombohedral packing has four contact points in the yield plane (which is four times as many as there are in the cubic packing), the probability of the particles in the rhombohedral packing being simultaneously separated from each other is much smaller than for particles in the cubic packing. Therefore, the particles in the loosest packing on the rupture plane will be easiest to separate from each other before complete breakage, and only the particles in the closest packing will yield the ultimate strength. However, some of their equations for the packing portions are ill posed since they assume that the yield plane of the powder sample is only composed of two kinds of particle portions, in cubic and

rhombohedral packing, R_c and R_r respectively, but the sum of the calculated portions, $R_c + R_r$, is not equal to unity.

4.6. Effect of the packing density on the tensile strength

The effect of the packing density or the void fraction of the powder mass on the tensile strength was investigated. We restate Eq. (8) here:

$$\sigma_{pz} = (1-\epsilon)\frac{k}{\pi}\frac{F_t}{d^2}$$

From Eqs. (3)–(7) and (9), we find

$$\frac{F_t}{\alpha d} = f(\delta, a/d, x_w, \epsilon) \qquad (15)$$

However, the dimensionless separation distance a/d is a constant and the contact angle δ can be assumed constant for a given liquid in contact with a given surface. Therefore, for a given moisture content x_w, $F_t/\alpha d$ or F_t is only a function of ϵ. However, the dependence on ϵ is very small since a change in the void fraction will only affect the coordination number or the number of liquid bridges in contact with each particle according to Eq. (9). This will slightly modify the size of the liquid bridge and barely affects the resulting attraction force. This is shown in Table 3 where the dimensionless attraction force is calculated at different void fractions. Therefore, F_t can be taken as constant and Eq. (8) can be rewritten as follows:

$$\sigma_{pz} = \frac{1-\epsilon}{\epsilon} K \qquad (16)$$

where K is a constant with units of N/m^2. Consequently, according to Eq. (16), if $\epsilon\sigma_{pz}$ is plotted as a function of $(1-\epsilon)$, the data points should lie on a straight line passing through the origin. Measurements were carried out on glass beads with 8.1% moisture over a range of void fractions from 0.42 to 0.58. The results are reported in Fig. 8 with data from other workers (the conditions under which these data have been obtained are listed in Table 4). At high solid fractions, a straight line can be drawn through each set of data, showing good linearity of $\epsilon\sigma_{pz}$ with $(1-\epsilon)$. For looser packings or small values of $(1-\epsilon)$, the data tend to curve down and the linearity no longer holds true. In any case, the straight lines do not go through the origin, proving that Eq. (8) proposed by Rumpf may not be correct and should be reconsidered. Rumpf based his model on several assumptions. First he only considered monosized particles, which may be an oversimplification. His theory only accounts partially for the effect of particle size because it does not allow for the probability of particles of different diameters to be in contact. Cheng [21,22] proposed a theory on the tensile strength of powders incorporating the effect of the powder density, the particle size distributions and an interparticle force which depends on the surface separation of particle pairs in the fracture plane. However, he has not been able to compare his model with the data of other workers and its complexity makes it impractical.

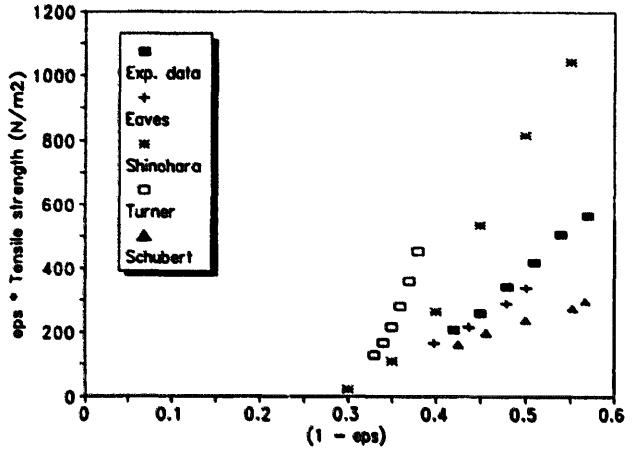

Fig. 8. $\epsilon\sigma_{pz}$ as a function of $1-\epsilon$ for glass beads 93 μm in diameter with a moisture content of 8.1% and for data from Eaves and Jones [19], Shinohara and Tanaka [6], Turner et al. [26] and Schubert [15].

Table 3
Dimensionless attraction force between particles bonded by a liquid bridge for different values of the void fraction ($a/d = 0.035$, $\delta = 0°$, $x_w = 8\%$)

ϵ	0.4	0.5	0.6	0.7
$F_t/\alpha d$	1.879	1.888	1.891	1.892

4.7. Effect of the heterogeneity of the packing on the tensile strength

Non-uniformity of the packing is not integrated into Rumpf's model either. However, according to Shinohara and Tanaka [6], it is believed that only particles in the dense

Table 4
Materials used by other workers and measurement conditions

Reference	Material	Size (μm)	Void fraction	Moisture or saturation
Eaves and Jones [19]	sodium chloride	54–302	0.499–0.602	$x_{w\,max} = 0.16$
Shinohara and Tanaka [6]	glass beads	23.8	0.47–0.70	$S = 0.047$–0.095
Turner et al. [26]	limestone	1.55	0.62–0.67	$x_w = 0.125$
Schubert and Wiboro [23]	glass beads	253	0.425–0.6	$S = 0.25$
Yokoyama et al. [25]	carboxymethyl cellulose	82	0.646–0.687	$S = 0.134$
Chan and Pilpel [24]	sodium chromoglycate	43	0.6–0.75	$x_w = 0.11$
Eaves and Jones [20]	lactose monohydrate glass beads	18	0.698–0.809	$x_w = 0.068$

Table 5
Tensile strength of heterogeneously packed samples with an overall void fraction of 0.52

Test no.		1	2	3	4
ϵ	bottom (7 mm)	0.43	0.46	0.49	0.52
	top (13 mm)	0.57	0.55	0.54	0.52
	overall (20 mm)	0.52	0.52	0.52	0.52
Tensile strength (N/m^2)		728.5	568.8	690.7	665.5

Table 6
Measured tensile forces (in gram-force) for the heterogeneously packed samples and the 7 mm samples

Void fraction at bottom of cell	0.43	0.46	0.49	0.52
Heterogeneous sample (7 mm + 13 mm)	120.3	93.9	114.1	108.7
7 mm sample	74.2	56.8	49.7	41.4
Ratio (%)	61.7	60.5	43.6	38.1

packing are responsible for the tensile strength of a powder. Experiments were performed in order to determine the tensile strength of heterogeneously packed samples. The bottom part of the cell was packed at different void fractions (0.43, 0.46, 0.49 and 0.52) over a height of 7 mm and the rest of the cell was filled with more powder in order to reach a total bed height of 20 mm and an overall void fraction of 0.52. The results are given in Table 5. It can be seen that the measured tensile strengths are different for each test even though the overall void fraction in the cell is the same. The value of the tensile strength is the highest for test 1 with the densest packing in the bottom of the cell. Except for test 2, the tensile strengths of the heterogeneously packed samples are higher than those of the homogeneously packed one. This shows that the tensile strength of a material depends on how the material is packed.

Next, experiments were conducted on samples with void fractions of 0.43, 0.46, 0.49 and 0.52 with a bed height of 7 mm. The tensile force needed to split the cell was recorded and compared with that required to break the heterogeneously packed samples in order to determine the contribution of the dense fraction to the tensile force. The ratio of the tensile force of the 7 mm sample to that of the heterogeneously packed one was also calculated. The results are shown in Table 6. The calculated ratios show that the dense packing fraction makes a large contribution to the tensile force and the highest ratio is for the highest packing. Table 6 also shows that the force needed to separate the cell is always greater for the heterogeneously packed sample with a bed height of 20 mm than for the 7 mm sample. This supports the fact that, contrary to Schubert's statement, the material in the upper part of the cell also contributes to the strength of the powder. Therefore, as mentioned earlier, it is reasonable to assume that the tensile strength does not vary with the bed height and that extrapolation to zero height is not necessary.

Finally, assuming that the tensile strength of the heterogeneously packed sample is a linear function of the tensile strengths of the two portions, the tensile strength was calculated from the tensile strengths measured in homogeneously packed samples, taking into account the respective sizes of the two portions in the fracture plane. Our measurements, which were performed on glass beads with a moisture content of 8.1%, are reported in Fig. 8. They were fit by the following relation:

$$\epsilon\sigma_{ps} = 2477(1-\epsilon) - 843 \quad (17)$$

The above relation allows for the calculation of σ_{ps} at the required values of ϵ. The calculated values are compared with those measured experimentally and the results are given in Table 7. Except for test 2, the calculated and measured values of the tensile strength match. This indicates that the tensile strength of a heterogeneously packed sample is a linear combination of the tensile strengths of the different portions present in the sample. This is not in agreement with the statement of Shinohara and Tanaka who claimed that only the densest packed fraction contributed to the ultimate tensile strength.

Table 7
Measured and calculated tensile strengths (in N/m^2) for heterogeneously packed samples

Test no.	1	2	3	4
Calculated	713.0	683.5	688.0	655.5
Measured	728.5	568.8	690.7	665.5

5. Universal correlation

It is difficult to derive a simple practical model which would predict the tensile strength of wet agglomerates in the pendular region. However, it may be possible to derive a simple correlation that would fit the experimental data available in the literature. A dimensionless analysis can show that the tensile strength is proportional to the bonding force and inversely proportional to the square of the particle diameter. Also, experimental measurements showed that it is also a function of the void fraction of the agglomerate. Therefore, the tensile strength is of the following form:

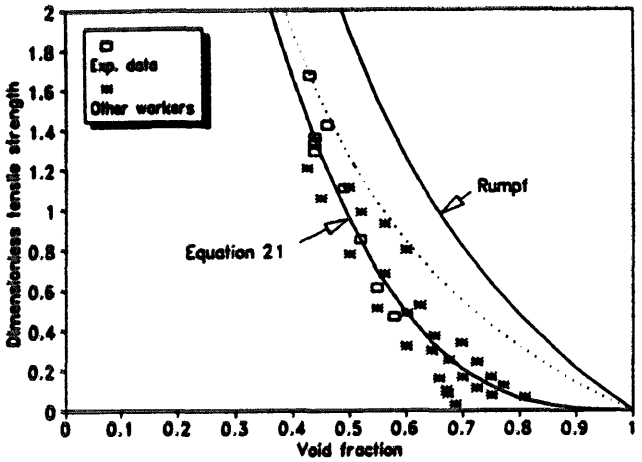

Fig. 9. Dimensionless tensile strength $\sigma a/d$ as a function of the void fraction ϵ for different powders with saturation in the plateau region of the pendular state.

$$\sigma_{pz} \sim f(\epsilon) \frac{F_t}{d^2} \tag{18}$$

Using Eq. (15),

$$\sigma_{pz} = \frac{\alpha}{d} f(\delta, a/d, x_w, \epsilon) \tag{19}$$

or, for the dimensionless tensile strength σ^*,

$$\sigma^* = \frac{\sigma_{pz} d}{\alpha} = f(\delta, a/d, x_w, \epsilon) \tag{20}$$

For a given wetting liquid, the contact angle δ is constant. a/d is also constant and therefore σ^* depends only on x_w and ϵ. Moreover, in the plateau region of the pendular state, the tensile strength and, therefore, σ^* do not vary when the moisture content is changed. Consequently, in the plateau region of the pendular state, σ^* is only a function of ϵ.

Data from different workers (see Table 4 for references, material characteristics and measurement conditions) were collected and $\sigma_{pz} d/\alpha$ was plotted as a function of ϵ for powders with saturation amounts in the plateau region of the pendular state as shown in Fig. 9. The data were fit by the following relation:

$$\sigma^* = \frac{\sigma_{pz} d}{\alpha} = 7.80(1-\epsilon)^{3.03} \tag{21}$$

Eqs. (8) and (9), derived from Rumpf's model, can be combined together to give

$$\sigma_{pz} = \frac{1-\epsilon}{\epsilon} \frac{F_t}{d^2} \tag{22}$$

Table 3 indicates that for a moisture content corresponding to the plateau region of the pendular state, the attraction force F_t is given by

$$F_t \approx 1.9 \alpha d \tag{23}$$

for a dimensionless separation distance $a/d = 0.035$ and is independent of the void fraction of the agglomerate.

The dimensionless tensile strength is then

$$\frac{\sigma d}{\alpha} \approx 1.9 \frac{1-\epsilon}{\epsilon} \tag{24}$$

and is also represented in Fig. 9. It can clearly be seen that Eq. (24) overpredicts the experimental data over the entire range of void fractions. The reason for this may be explained as follows. In his derivation, Rumpf considered bonding forces distributed uniformly over all the directions in the space, which corresponds to an isostatic stress in the granule. In this case, the principal stresses are equal and collapse to one point A in Fig. 10 which shows the linear yield locus of a sample in the region of negative normal stresses. On the other hand, point B represents uniaxial stress conditions which are encountered during tensile strength measurements when one principal stress acts in the horizontal direction while the other principal stress in the vertical direction is zero (free surface). The uniaxial tensile strength σ_1 is linked to the isostatic tensile strength σ_2 by the following relation derived from the geometry of Fig. 10:

$$\sigma_2 = \frac{1+\sin\phi}{2\sin\phi} \sigma_1 \tag{25}$$

where ϕ is the angle of internal friction in the bulk. For most powders, values of ϕ are close to 30°. Therefore, $\sigma_2 \approx 1.5\sigma_1$, or the uniaxial tensile stress is usually one and a half times smaller than the isostatic tensile stress. The dimensionless uniaxial tensile strength is represented by the dotted line in Fig. 9 and now lies somewhat closer to the experimental data points.

The proposed correlation allows for the calculation of the tensile strength of a powder in the plateau region of the pendular state from the knowledge of parameters which are easy to measure. The tensile strength of powders with a moisture content or saturation level less than that corresponding to the plateau region can be extrapolated if one assumes that it is proportional to the bonding force defined in Eq. (5). In the plateau region, the dimensionless bonding force $F_t/d\alpha$ is about 1.89 (see Fig. 11) for $a/d = 0.035$ and $\delta = 0°$. At a lower saturation level, the dimensionless volume of the liquid bridge, V_{bridge}/d^3, can be calculated using Eqs. (6), (9) and

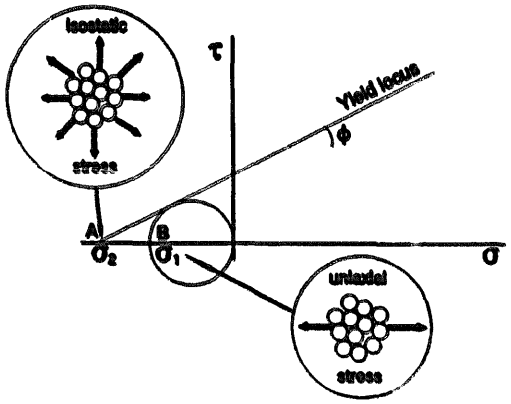

Fig. 10. Uniaxial and isostatic tensile stresses.

Table 8
Tensile strength of powders at low saturation derived from Eq. (21): comparison with experimental values

Workers	Material	d_p (μm)	ϵ	σ^* from Eq. (21)	Sat. (%)	θ	F^* from Fig. 11	σ^*	σ	σ_{exp}	Error (%)
Pierrat	glass beads	93	0.45	1.2725	2.4	18.5	1.420	0.954	739.0	692	+6.8
					4.8	23.7	1.675	1.126	871.7	849	+2.7
Schubert	limestone	71	0.415	1.5343	2.2	16.5	1.278	0.989	1002.8	1606	−37.6
					4.7	21.8	1.595	1.293	1311.0	2176	−39.8
					7.7	26.0	1.745	1.414	1434.3	2500	−42.6
Pietsch	limestone	13	0.50	0.9531	1.6	17.9	1.382	0.696	3854	4254	+9.4
					4.8	26.7	1.758	0.885	4902	5981	−18.0
Eaves and Jones	sodium chloride	127	0.499	0.9589	4.7	26.5	1.750	0.886	502.6	472.1	+6.5
					7.4	31.0	1.835	0.929	527.0	646.1	−18.4
Eaves and Jones	sodium chloride	127	0.521	0.8369	4.3	26.8	1.761	0.778	441.4	401.2	+10.0
					6.8	31.5	1.841	0.814	461.4	545.8	−15.5
Eaves and Jones	sodium chloride	127	0.563	0.6336	3.7	27.5	1.777	0.595	337.2	295	+14.3
					6.1	33.0	1.859	0.622	352.7	385	−8.4
Eaves and Jones	sodium chloride	127	0.543	0.7260	4.0	27.3	1.772	0.679	385.1	378.3	+1.8
					6.2	32.0	1.847	0.708	401.4	503.3	−20.2
Eaves and Jones	glass	18	0.809	0.0515	1.2	32.2	1.849	0.050	201.2	158.1	+27.3
Eaves and Jones	glass	18	0.749	0.1179	1.7	31.2	1.840	0.1146	458.5	490.5	−6.5
Eaves and Jones	glass	18	0.698	0.2066	1.9	30.5	1.829	0.1996	798.6	1033.1	−22.7

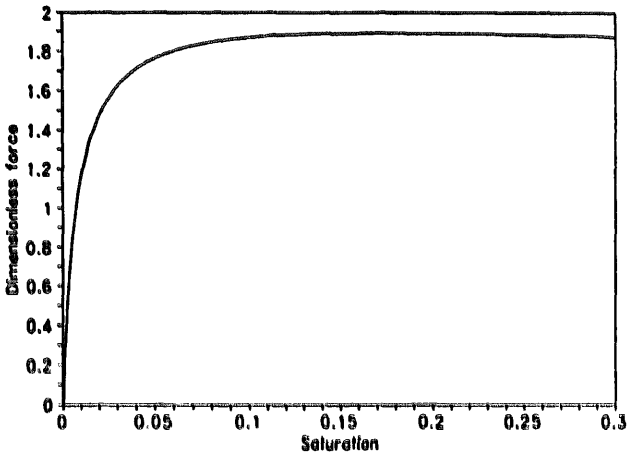

Fig. 11. Dimensionless force as a function of saturation ($a/d=0.035$ and $\delta=0°$).

(13), provided that ϵ is known. Then Eq. (7), combined with Eqs. (3), (4) and (5), gives the dimensionless bonding force corresponding to the saturation level considered. It can also be read directly from Fig. 11. This value is divided by 1.89 and this correction factor is used to calculate the tensile strength of the powder at the saturation level of interest. Some calculations were performed for different powders of various sizes, void fractions and moisture contents [6,15,18–20,23–26]. The results are shown in Table 8. Errors appearing in the calculated tensile strength at low saturation are in the range ±20%, which is reasonably good. This shows that Eq. (21), which gives the dimensionless tensile strength of powders with saturations in the plateau region, can also be used to find the tensile strength of a powder at any saturation in the pendular region.

It should also be mentioned that in the capillary state the dimensionless tensile strength can be obtained from Eqs. (11) and (12), proposed by Schubert [15]. Moreover, in the pendular region the dimensionless tensile strength can also be calculated from Eq. (14) using correlation Eq. (21) and Eqs. (11) and (12) put in dimensionless form, provided that S_c and S_f are known. S_c is generally taken equal to 90% and S_f can be calculated using the derivation of Flemmer [17].

Therefore, the tensile strength of wet granular materials at any saturation can be conveniently obtained from the proposed correlation and the equations derived by Schubert [15] and easy-to-measure parameters.

6. Conclusions

The tensile strength of granular materials can be measured experimentally or calculated from correlations found in the literature. Direct measurements are always subject to experimental errors which can be significant for powders with low tensile strengths, and reproducibility of the measurements can be poor in some cases. Therefore, models predicting the tensile strength of granular materials are very useful. However, results of experimental measurements carried out on glass beads did not compare well with the values of the tensile strength predicted by Rumpf's model. The correlation also failed to match experimental data from other workers who conducted tests on various powders.

The data were fit with a simple correlation which gives the dimensionless tensile strength of powders in the plateau region of the pendular state as a function of the void fraction of the agglomerate. The tensile strength of powders with saturations below the plateau region can be calculated assuming proportionality to the bonding force due to the liquid bridges. This force depends on the dimensionless separation distance between the particles, which cannot be measured. However, the profile of the tensile strength versus saturation

suggests that $a/d = 0.035$. In the funicular state the tensile strength can also be determined from Eq. (21), provided that the capillary pressure and the transition saturation S_f between the pendular and the funicular state are known. However, the value of S_f cannot always be computed accurately because the transition between the pendular and the funicular state is not always clearly defined. This is particularly true for polydispersed powders.

The tensile strength of a wet granular material is a strong function of the packing density. Local differences in the void fraction affect the strength of the material and the densest fraction in the agglomerate contributes the most to its strength. The scatter of the data in Fig. 9 shows that, for a given value of the void fraction, there is a large variation in the corresponding tensile strength. The packing density of the material must be measured accurately in order to minimize the uncertainty when using the correlation. Void fraction measurements are easy to perform, and it was found that for wet glass beads the measurements were reproducible and the experimental error is usually small.

Eq. (21) gives the tensile strength of powders wetted with liquid with zero contact angle. For contact angles less than 20°–30°, the proposed correlation is believed to give reasonably accurate results. However, for hydrophobic particles the bonding force is greatly reduced and the correlation will overpredict the actual value of the tensile strength.

The correlation for the tensile strength requires knowledge of the particle diameter, the surface tension of the wetting liquid and the void fraction of the agglomerate. In the case of polydispersed powders, a clear choice of average particle diameter is not yet available and more data are needed to evaluate the correlation. Efforts [21,22] to integrate the effect of the particle size distribution in a model have yielded complicated correlations not yet supported by experiments.

7. List of symbols

a separation distance
a' ≈6 to 8
d particle diameter
F_c force due to curvature of liquid bridge
F_s force due to surface tension
F_t resulting force
h radius of curvature of liquid bridge
h^* dimensionless radius of curvature of liquid bridge
k mean coordination number
K constant in Eq. (16)
m_{liq} mass of liquid
m_{sol} mass of dry particle
p_c capillary pressure
r_1 radius of curvature of liquid bridge
r_1^* dimensionless radius of curvature of liquid bridge
S saturation
S_c saturation at transition between funicular and capillary states
S_f saturation at transition between pendular and funicular states
V_{liq} volume of liquid
V_{sol} volume of dry particle
x_w moisture content

Greek letters

α surface tension
δ contact angle
ϵ volume void fraction
θ filling angle
ρ_{liq} liquid density
ρ_{sol} particle density
σ^* dimensionless tensile strength
σ_{cz} tensile strength in capillary state
σ_{fz} tensile strength in funicular state
σ_{pz} tensile strength in pendular state
σ_1 uniaxial tensile strength
σ_2 isostatic tensile strength
ϕ angle of internal friction

Acknowledgements

Support from New York State Electric and Gas and the Petroleum Research Fund is gratefully acknowledged.

References

[1] J.G. Dawes, *Saf. Mines Res. Estab. Res. Rep. 36*, HMSO, London, 1952.
[2] H.S. Eisner, G. Fogg and T.W. Taylor, *3rd Int. Congr. Surface Activity, Vol. 2*, 1960, pp. 378–382.
[3] G. Thouzeau and T.W. Taylor, *Saf. Mines Res. Estab. Res. Rep. 197*, HMSO, London, 1962.
[4] M.D. Ashton, R. Farley and F.H.H. Valentin, *J. Sci. Instrum., 41* (1964) 763–765.
[5] P.A. Hartley and G.D. Parfitt, *J. Phys. E.: Sci. Instrum., 17* (1984) 347–349.
[6] K. Shinohara and T. Tanaka, *J. Chem. Eng. Jpn., 8* (1975) 46–50.
[7] S. Yano, H. Shiramise, K. Hayashida and M. Arakawa, *Proc. Spring Meet. Soc. Powder Technol. Jpn., 1979*, p. 78.
[8] R.B. Heady and J.W. Cahn, *Metall. Trans., 1* (1970) 185–189.
[9] V.P. Mehrotra and K.V.S. Sastry, *Powder Technol., 25* (1980) 203–214.
[10] W.B. Pietsch and H. Rumpf, *Chem. Ing. Tech., 39* (1967) 885–893.
[11] H. Schubert, *Powder Technol., 11* (1975) 107–119.
[12] H. Rumpf, in W.A. Knepper (ed.), *Agglomeration*, Interscience, New York, 1962, p. 379.
[13] H. Rumpf, *Chem. Ing. Tech., 30* (1958) 144.
[14] W.O. Smith, P.D. Foote and P.F. Busang, *Phys. Rev., 34* (1929) 1271–1274.
[15] H. Schubert, *Chem. Ing. Tech., 45* (1973) 396–401.
[16] H. Schubert, *Thesis*, University of Karlsruhe, Germany, 1972.
[17] C.L. Flemmer, *Powder Technol., 66* (1991) 191–194.
[18] W. Pietsch, E. Hoffman and H. Rumpf, *Ind. Eng. Chem. Prod. Res. Dev., 8* (1969) 58–62.
[19] T. Eaves and T.M. Jones, *J. Pharm. Sci., 61* (1972) 256–261.

[20] T. Eaves and T.M. Jones, *J. Pharm. Sci.*, *61* (1972) 342–348.
[21] D.C.H. Chang, *Chem. Eng. Sci.*, *23* (1968) 1405–1420.
[22] D.C.H. Chang, *J. Adhesion*, *2* (1970) 82–92.
[23] H. Schubert and W. Wiboro, *Chem. Ing. Tech.*, *42* (1970) 541–545.
[24] S.Y. Chan and N. Pilpel, *J. Pharm. Pharmacol.*, *35* (1983) 477–481.
[25] T. Yokoyama, K. Fujii and T. Yokoyama, *Powder Technol.*, *32* (1982) 55–62.
[26] G.A. Turner, M. Balasubramanian and L. Otten, *Powder Technol.*, *15* (1976) 97–105.